

# An Attention and Prediction Guided Visual System for Small Target Motion Detection in Complex Natural Environments

Hongxin Wang, Jiannan Zhao, Huatian Wang, Jigen Peng, and Shigang Yue, *Senior Member, IEEE*

**Abstract**—Small target motion detection within complex natural environment is an extremely challenging task for autonomous robots. Surprisingly, visual systems of insects have evolved to be highly efficient in detecting mates and tracking prey, even though targets are as small as a few pixels in visual field. The excellent sensitivity to small target motion relies on a class of specialized neurons called small target motion detectors (STMDs). However, existing STMD-based models are heavily dependent on visual contrast and perform poorly in complex natural environment where small targets always exhibit extremely low contrast to neighboring backgrounds. In this paper, we propose an attention and prediction guided visual system to overcome this limitation. The proposed visual system mainly consists of three subsystems, including an attention module, a STMD-based neural network, and a prediction module. The attention module searches for potential small targets in the predicted areas of input image and enhances their contrast to complex background. The STMD-based neural network receives the contrast-enhanced image and discriminates small moving targets from background false positives. The prediction module foresees future positions of the detected targets and generates a prediction map for the attention module. The three subsystems are connected in a recurrent architecture allowing information processed sequentially to activate specific areas for small target detection. Extensive experiments on synthetic and real-world datasets demonstrate the effectiveness and superiority of the proposed visual system for detecting small, low-contrast moving targets against complex natural environment.

**Index Terms**—Bioinspiration, small target motion detection, prediction, robotic visual perception, complex natural environment.

## I. INTRODUCTION

IN visual world, object motion provides important information to guide the behavior of observers (animals or robots). Future autonomous systems should be able to operate in complex dynamic environment, detecting object motion, understanding movement intention, predicting future path, and reacting properly. It is known that detecting potentially dangerous objects early and in the distance would allow sufficient time for autonomous systems to make responses, so as to

This work was supported in part by EU HORIZON 2020 Project STEP2DYNA under Grant 691154, in part by EU HORIZON 2020 Project ULTRACEPT under Grant 778062, and in part by the National Natural Science Foundation of China under Grant 11771347 and Grant 12031003. (Corresponding author: Shigang Yue & Jigen Peng.)

Ho. Wang, J. Zhao, Hu. Wang, and S. Yue are with the Computational Intelligence Lab, School of Computer Science, University of Lincoln, Lincoln LN6 7TS, U.K. (email: syue@lincoln.ac.uk).

J. Peng is with the School of Mathematics and Information Science, Guangzhou University, Guangzhou 510006, China (email: jgpeng@gzhu.edu.cn).



Fig. 1. Examples of small moving targets [1]. (a) A unmanned aerial vehicle (UAV), and (b) a bird in the distance where their surrounding regions are enlarged in the red boxes. Both the UAV and bird appear as dim speckles with only a few pixels in size where most of visual features are difficult to discern. In particular, they all show extremely low contrast against the complex background.

maintain a dominant position in interaction/competition. If an object is extremely small or distant from the observer, it always appears as a small dim speckle on image with only one or a few pixels in size, where most of visual features are difficult to identify, for example, a unmanned aerial vehicle (UAV) or a bird in the distance, as illustrated in Fig. 1.

Small target motion detection plays a critical role in a number of computer vision tasks, including video surveillance, early warning, visual tracking and defences. For example, timely finding micro drones flying over the runways would protect airports from disruption. However, discriminating small moving targets against complex natural environment remains challenging to artificial visual systems. This is because: 1) small targets always equate to only a few pixels in images, with low-resolution appearance and unclear structure, and most of visual features, such as color, orientation, and texture, are difficult to discern, which means feature representations of small targets for motion detection are extremely weak; 2) small targets exhibit blurred boundaries and low contrast to heavily cluttered backgrounds, which makes them difficult to distinguish from noisy clutter; 3) freely moving camera could introduce complex changing scene and relative motion to small targets, which bring further challenges to motion discrimination.

Conventional approaches for motion detection can be classified into three main categories: frame difference [2], background subtraction [3], and optical flow [4]. These approaches work best for static cameras, but their performance decreases significantly in the applications involving mobile cameras, such as autonomous driving systems, flying drones, and mobile robots. In addition, these approaches cannot be directly applied to small target detection in complex natural environment,

because: 1) they are unable to discriminate small targets from large objects in images, for example, pedestrian and/or vehicles; 2) small targets are always hidden in pixel errors and background noise after applying camera motion compensation. Appearance-based methods can also be adopted for motion detection by extracting low-to-high level visual features to classify moving objects based on machine learning algorithms, such as convolutional neural networks [5], support vector machines [6] and evolutionary computation [7]. However, these methods are ineffective against small objects with only a few pixels in size, since most of visual features are difficult to identify from their low-resolution appearance.

Learning from the animals' visual systems is a promising way to build effective and robust models for detecting small moving targets in complex natural environment [8]–[10]. Despite the fact that the neural circuits in insects are relatively simpler than those in human brains, insects achieve a extremely high successful rate of 97% in pursuing small flying mates or prey. The exquisite sensitivity of insects to small moving targets is supported by a class of specialized neurons called small target motion detectors (STMDs) [11]–[13]. More precisely, STMD neurons respond strongly to moving objects as small as  $1^\circ - 3^\circ$  of the visual field, while exhibiting much weaker or even no response to large objects typically occupying larger than  $10^\circ$ . In addition, the STMD neural responses are robust even when small targets display extremely low contrast to cluttered moving backgrounds. Understanding neural computation that underlies small target motion detection would provide inspirations for how similar problems can be solved in autonomous systems.

Motivated by the superior properties of STMD neurons, several attempts have been made to develop quantitative STMD-based models for small target motion detection. Wiederman *et al.* [14] proposed an Elementary STMD model (ESTMD) to detect the presence of small moving targets by multiplying luminance increase and decrease signals at each pixel after lateral inhibition. To determine motion direction of small targets, the cascaded model [15] and Directionally Selective STMD (DSTMD) [16] were developed by considering the correlation of luminance change signals from two different pixels. Wang *et al.* [17] proposed a visual system called STMD Plus, which takes into account both motion information and directional contrast, to filter out false positives in cluttered moving backgrounds. However, these models are heavily reliant on contrast between small targets and the background. Specifically, their detection performance will degrade significantly as the decrease of target contrast. In complex natural environment where small targets always exhibit extremely low contrast, it is arduous for these models to discern small target motion effectively and robustly.

To overcome the aforementioned limitation, we develop an attention and prediction guided visual system (called apg-STMD). Prediction and attention are fundamental functions in insects' visual systems, where the former utilizes present and/or past information to anticipate future object motion, while the latter prioritizes objects of interest amidst a swarm of potential alternatives [18]–[21]. In the proposed visual system, an attention module and a prediction module are connected

with a STMD-based neural network in a recurrent architecture. Specifically, at each time step, the input image and a prediction map are applied to the attention module to search for potential small targets in several predicted areas. A contrast-enhanced image is produced by enhancing the contrast of potential targets over the input image, and then fed into the STMD-based neural network for discriminating small moving targets. The prediction module anticipates future positions of the detected small targets and generates a prediction map which is propagated to the attention module in the next time step. Experiments demonstrate the superior performance of the proposed visual system in detecting small target motion against complex backgrounds.

The rest of this paper is organized as follows. Section II discusses the related work for motion-sensitive neural models, attention and prediction mechanisms. We describe the proposed attention and prediction guided visual system in Section III. The experimental results on both synthetic and real-world data sets are reported in Section IV. Finally, Section V concludes this paper.

## II. RELATED WORK

### A. Motion-sensitive Neural Models

Lobula giant movement detector (LGMD) [22], [23], lobula plate tangential cell (LPTC) [24], [25], and small target motion detector (STMD) [11]–[13] are three widely investigated motion-sensitive neurons. The LGMD responds most strongly to approaching objects, but shows little or no response to receding objects. It has been modelled as a collision detector that is further embodied in micro mobile robots [26]–[29] and UAVs [30], [31] for collision avoidance. The LPTC is sensitive to objects which occupy a wide region of the visual field and move along preferred directions. A wide-field LPTC can be modelled by an array of Hassenstein-Reichardt correlators [32], each of which focuses on a small part of the visual field. The LPTC model has been used for velocity estimation [33], collision avoidance [34], and object tracking [35]. Although the LGMD and LPTC models perform well in detecting collision and wide-field motion, they are unable to discriminate small targets from other large objects in the visual field.

The STMD gives peak responses to small target motion, but much weaker or even no response to wide-field motion and background movement. The STMD-based models, such as ESTMD [14], the cascaded model [15], DSTMD [16], and STMD Plus [17], have been developed to discriminate small moving targets against complex backgrounds. However, these models are all sensitive to contrast of small targets and perform poorly in complex dynamic environment where small target always exhibit extremely low contrast to their neighboring backgrounds.

### B. Attention Mechanism

Attention mechanism is fundamentally important for animals to forage, avoid predators, and search for mates, which focuses limited computation resources on parts of visual field [18]. For example, bumblebees are able to select flowers of

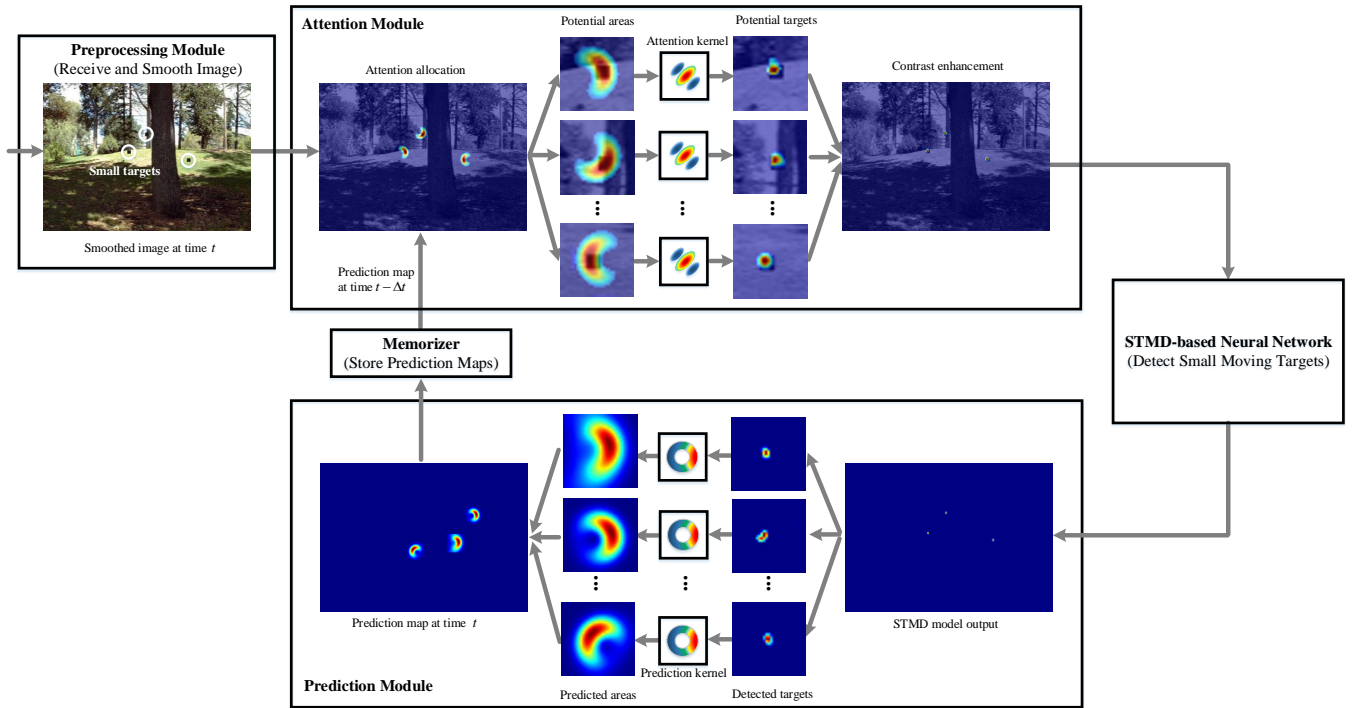


Fig. 2. Overall flowchart of the proposed attention and prediction guided visual system. It consists of a preprocessing module (left), an attention module (top), a STMD-based neural network (right), a prediction module (bottom), and a memorizer (middle).

particular colours, while ignoring differently coloured distractors during visual search [36]; Drosophila selectively fixate on the most salient one in the swarms of prey and conspecifics that display different contrast against complex background [37]; fiddler crabs adjust their escape behaviour and selectively suppress neural responses to less dangerous predators when confronted with multiple threats in order to minimise the combined risk [20].

Attention has been popularly employed in various tasks, such as image classification [38], visual question answering [39], natural language processing [40], and image captioning [41], to boost model performance by adaptively choosing a sequence of regions for fine processing. However, it has not been utilized in artificial visual systems to detect small moving targets against complex natural backgrounds. Moreover, the interaction of attention with prediction mechanisms for small target motion detection has not been deeply investigated.

### C. Prediction Mechanism

Prediction mechanism plays an important role in insects' visual systems, which anticipates future positions of prey and mates, but also contributes to path planning during rapid pursuit [42]. Recent research [21] reveals that prediction process is able to enhance localized sensitivity to a small target ahead of its motion path, while exhibiting suppression elsewhere. Furthermore, when the target is occluded or abruptly disappears, the localized sensitivity will move forward and gradually weaken over time.

The ability to model animals' prediction mechanisms and use them to understand object motion in complex environment is extremely valuable for a wide ranges of applications. For

example, reliable prediction of surround object motions (e.g., vehicles, pedestrians and cyclists) is a key technology for safe advanced autonomous driving [43]; keeping track of current and future motion states of people is critical for socially-aware robots to avoid collision in populated environments [44]; nursing-care assistant robots should be able to automatically anticipate human intentions by their actions to improve coordination [45]. However, little work has been done on modeling prediction mechanisms to anticipate small target motion against complex natural backgrounds.

## III. ATTENTION AND PREDICTION GUIDED VISUAL SYSTEM

The proposed visual system is composed of five subsystems, including three modules (i.e., preprocessing, attention, prediction), a STMD-based neural network, and a memorizer, as illustrated in Fig. 2. Once an image is received at time  $t$ , it is first smoothed by the preprocessing module, then applied to the attention module to determine several potential areas based on the prediction map from the memorizer. In each area, potential small targets are selected by convolution with the attention kernels and their contrast to background are enhanced by addition of the convolutional outputs. The contrast-enhanced image is fed into the STMD-based neural network for discriminating small moving targets from complex background. In the prediction module, futures positions of the detected targets at time  $t + \Delta t$  are anticipated by convolution with the prediction kernels, then merged into a prediction map that is stored in the memorizer for next input image. We describe network architecture of the proposed visual system

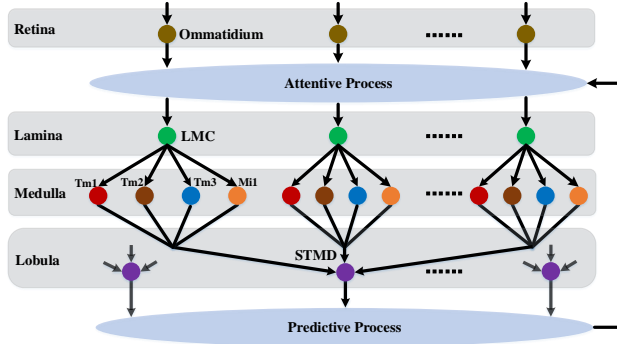


Fig. 3. Network architecture of the proposed attention and prediction guided visual system, where each colored circular node denotes a neuron.

in Section III-A, then elaborate on its components in Section III-B – III-E.

#### A. Network Architecture of the Proposed Visual System

To realize the functions in Fig. 2, a number of specialized neurons are coordinated together in the proposed visual system whose network architecture is shown in Fig. 3. As can be seen, the proposed visual system consists of four neural layers, including retina, lamina, medulla, and lobula [46], where an attention and a prediction mechanisms are implemented on the outputs of the retina and lobula, respectively. Specifically, ommatidia [47] capture and preprocess visual information from the whole scene, then the attention is allocated to parts of the visual scene to enhance signals of potential small targets. The enhanced signals are applied to large monopolar cells (LMCs) [48], further parallelly processed by four medulla neurons (i.e., Tm1, Tm2, Tm3, and Mi1) [49], finally integrated in the STMDs to detect small moving targets against complex backgrounds. Future positions of the detected targets are predicted and then fed back to the attentive process.

#### B. Preprocessing Module

The preprocessing module contains numerous ommatidia that are arranged in matrix form to receive an entire image as model input. The luminance of each pixel is captured by each ommatidium and then smoothed by convolution with a Gaussian kernel. Formally, we represent input image by  $I(x, y, t) \in \mathbb{R}$  where  $(x, y)$  is spatial coordinates and  $t$  denotes time. Given a Gaussian kernel with standard deviation  $\sigma_1$

$$G_{\sigma_1}(x, y) = \frac{1}{2\pi\sigma_1^2} \exp\left(-\frac{x^2 + y^2}{2\sigma_1^2}\right) \quad (1)$$

then the output of an ommatidium  $P(x, y, t)$  is defined as

$$P(x, y, t) = \iint I(u, v, t) G_{\sigma_1}(x - u, y - v) du dv. \quad (2)$$

#### C. Attention Module

As can be seen from Fig. 2, a smoothed image  $P(x, y, t)$  and a prediction map  $M(x, y, t - \Delta t)$  form the inputs of the attention module. A set of potential areas denoted as  $\{\Omega_i | i = 1, 2, \dots, N\}$  is first determined by comparing  $M(x, y, t - \Delta t)$

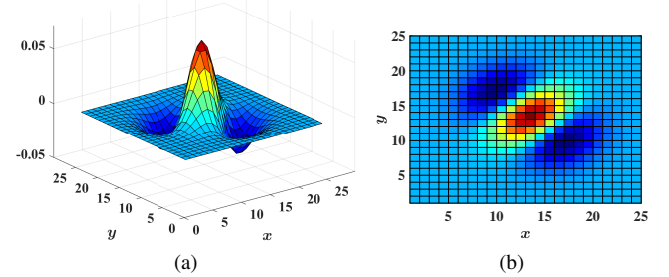


Fig. 4. (a) Three-dimensional and (b) planar representations of an attention kernel  $W_a(x, y, \varsigma, \theta)$  where  $\varsigma = 3.0$ ,  $\theta = \pi/4$ .

with a threshold. To search for potential small targets in each area  $\Omega_i$ , the attention module convolves  $\Omega_i$  with a family of attention kernels. Let  $\Sigma$  and  $\Theta$  denote sets of scale and orientation, respectively, then an attention kernel is defined as

$$W_a(x, y, \varsigma, \theta) = 2 \frac{\varsigma^2 - (x \cos \theta + y \sin \theta)^2}{\pi \varsigma^4} \exp\left(-\frac{x^2 + y^2}{2\varsigma^2}\right) \quad (3)$$

where scale  $\varsigma \in \Sigma$  and orientation  $\theta \in \Theta$ . As shown in Fig. 4, the attention kernel measures the luminance difference between the central part and surrounding areas on both sides along the orientation  $\theta$ . Since a small target always displays speckle-like structure in image whose luminance is higher or lower than that of its surrounding background, a significant response will appear at the target position after the convolution with an attention kernel. To suppress non-speckle structures, such as lines, edges, and corners, we select the minimal convolution output by varying kernel orientation  $\theta$  for each scale  $\varsigma$ , then obtain the maximal output among all the scales [50], that is

$$A_i(x, y, t) = \max_{\varsigma \in \Sigma} \min_{\theta \in \Theta} \iint_{\Omega_i} P(u, v, t) W_a(x - u, y - v, \varsigma, \theta) du dv \quad (4)$$

where  $A_i(x, y, t)$  denotes the response of the attention module in the local area  $\Omega_i$ . To enhance the contrast of the potential target to its surrounding background, we add  $A_i(x, y, t)$  with the smoothed image  $P(x, y, t)$ , that is

$$P_e(x, y, t) = P(x, y, t) + \alpha \sum_{i=1}^N A_i(x, y, t) \quad (5)$$

where  $P_e(x, y, t)$  denotes the contrast-enhanced image,  $\alpha$  is a constant, and  $N$  is the number of the local areas  $\Omega_i$ .

#### D. STMD-based Neural Network

The STMD-based neural network is composed of three sequentially arranged neural layers, including lamina, medulla, and lobula, as shown in Fig. 3. To detect small moving targets against complex natural background, the contrast-enhanced image  $P_e(x, y, t)$  from the attention module is processed by the LMCs, medulla neurons, and STMDs in a feedforward manner.

1) *Large Monopolar Cells*: Luminance of a pixel will change over time when an object passes through it. To measure temporal luminance changes of each pixel, we model the LMC as a band-pass filter in time domain (see Fig. 5). Its impulse

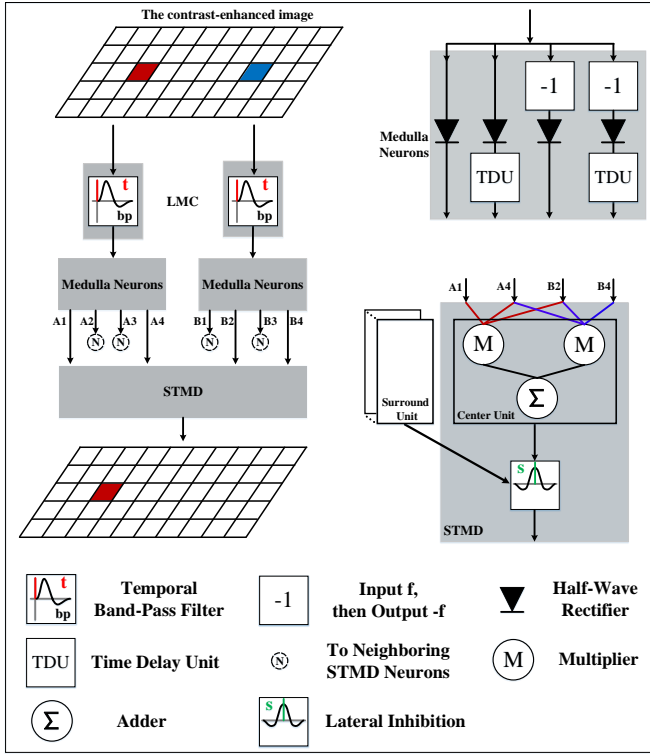


Fig. 5. Schematic of the STMD-based neural network. At each time step, it receives an entire contrast-enhanced image from the attention module which is processed by the LMCs, medulla neurons, and STMDs sequentially. Note that only a STMD and its pre-synaptic neurons are presented here for better visualization, but they are all arranged in matrix form.

response  $H(t)$  is defined by the difference of two Gamma kernels [51], namely

$$H(t) = \Gamma_{n_1, \tau_1}(t) - \Gamma_{n_2, \tau_2}(t) \quad (6)$$

$$\Gamma_{n, \tau}(t) = (nt)^n \frac{\exp(-nt/\tau)}{(n-1)! \cdot \tau^{n+1}} \quad (7)$$

where  $\Gamma_{n, \tau}(t)$  denotes a Gamma kernel with order  $n$  and time constant  $\tau$ . The output of a LMC is given by convolving  $H(t)$  with the contrast-enhanced image  $P_e(x, y, t)$

$$L(x, y, t) = \int P_e(x, y, s) H(t-s) ds \quad (8)$$

where  $L(x, y, t)$  denotes the output of the LMC corresponding to pixel  $(x, y)$  at time  $t$ . Note that  $L(x, y, t)$  reveals changes in luminance at pixel  $(x, y)$  with respect to time  $t$ . Specifically, a positive output means an increase in luminance whereas a negative one reflects a decrease.

2) *Medulla Neurons*: Four medulla neurons, including Tm1, Tm2, Tm3, and Mi1, are connected to a single LMC and process the LMC output  $L(x, y, t)$  in parallel, as can be seen from Fig. 3. Specifically, the Tm3 neuron is modelled as a half-wave rectifier to allow the positive part of  $L(x, y, t)$  while blocking the negative part; in contrast, the Tm2 neuron allows the negative part and blocks the positive part. Denote

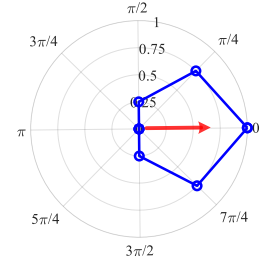


Fig. 6. Normalized outputs of the STMD neuron to a small target at pixel  $(x_0, y_0)$  and time  $t_0$  along eight preferred directions  $\theta \in \{0, \frac{\pi}{4}, \frac{\pi}{2}, \frac{3\pi}{4}, \pi, \frac{5\pi}{4}, \frac{3\pi}{2}, \frac{7\pi}{4}\}$ . The red arrow denotes the motion direction of the object.

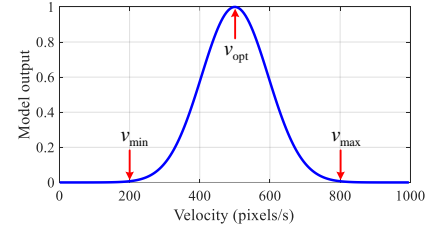


Fig. 7. Normalized outputs of the STMD neuron to small targets with different velocities.  $[v_{\min}, v_{\max}]$  and  $v_{\min}$  denote the preferred velocity range and the optimal velocity of the STMD, respectively.

the output of Tm3 and Tm2 by  $S^{Tm3}(x, y, t)$  and  $S^{Tm2}(x, y, t)$ , respectively, and then they are given by

$$S^{Tm3}(x, y, t) = [L(x, y, t)]^+ \quad (9)$$

$$S^{Tm2}(x, y, t) = [-L(x, y, t)]^+ \quad (10)$$

where  $[x]^+$  refers to  $\max(x, 0)$ . As shown in Fig. 5, the Mi1 and Tm1 neurons serve as half-wave rectifiers followed with a time-delay unit (TDU) where temporal delay is implemented by convolution with a Gamma kernel, that is

$$S_{(n, \tau)}^{Mi1}(x, y, t) = \int [L(x, y, s)]^+ \cdot \Gamma_{n, \tau}(t-s) ds \quad (11)$$

$$S_{(n, \tau)}^{Tm1}(x, y, t) = \int [-L(x, y, s)]^+ \cdot \Gamma_{n, \tau}(t-s) ds \quad (12)$$

where  $S_{(n, \tau)}^{Mi1}(x, y, t)$  and  $S_{(n, \tau)}^{Tm1}(x, y, t)$  denote the outputs of the Mi1 and Tm1 neurons, respectively; order  $n$  and time constant  $\tau$  of Gamma kernel  $\Gamma_{n, \tau}(t)$  control the time-delay order and length, respectively.

3) *Small Target Motion Detectors*: Medulla neurons located at two different pixels provide inputs to a STMD neuron, as illustrated in Fig. 5. The two pixels denoted by  $(x, y)$  and  $(x'(\theta), y'(\theta))$ , respectively, are defined as

$$\begin{aligned} x'(\theta) &= x + \gamma \cdot \cos \theta \\ y'(\theta) &= y + \gamma \cdot \sin \theta \end{aligned} \quad (13)$$

where  $\theta$  stands for the preferred direction of the STMD,  $\gamma$  denotes a constant. Note that when an object moves from pixel  $(x, y)$  to  $(x'(\theta), y'(\theta))$ , it will induce increase and decrease in luminance of the two pixels. The luminance-change information have been captured by the LMCs, further separated into increase and decrease parts by the four medulla neurons. To produce a significant response to the moving object, the

STMD first aligns these luminance-increase and luminance-decrease signals correctly in time domain, then multiplies the temporally-aligned signals together [16], that is

$$D(x, y, t, \theta) = S^{\text{Tm}3}(x, y, t) \times \left\{ S_{(n_4, \tau_4)}^{\text{Tm}1}(x, y, t) + S_{(n_3, \tau_3)}^{\text{Mi}1}(x'(\theta), y'(\theta), t) \right\} \times S_{(n_5, \tau_5)}^{\text{Tm}1}(x'(\theta), y'(\theta), t) \quad (14)$$

where  $D(x, y, t, \theta)$  represents the output of the STMD with a preferred direction  $\theta$ ; the time constants, i.e.,  $\tau_3$ ,  $\tau_4$ , and  $\tau_5$ , are determined by time intervals between the luminance-increase and decrease signals of the two pixels; the orders, i.e.,  $n_3$ ,  $n_4$ , and  $n_5$ , control the shapes of signals after temporal alignment.

The correlation output  $D(x, y, t, \theta)$  is further convolved with two inhibition kernels, including  $W_s(x, y)$  in spatial domain for suppressing responses to large moving objects, and  $W_d(\theta)$  in direction domain for inhibiting responses more than  $45^\circ$  apart, which are defined as

$$W_s(x, y) = A \cdot [g(x, y)]^+ + B \cdot [g(x, y)]^- \quad (15)$$

$$g(x, y) = G_{\sigma_2}(x, y) - e \cdot G_{\sigma_3}(x, y) - \rho \quad (16)$$

$$W_d(\theta) = G_{\sigma_4}(\theta) - G_{\sigma_5}(\theta) \quad (17)$$

where  $[x]^+$  and  $[x]^-$  refer to  $\max(x, 0)$  and  $\min(x, 0)$ , respectively;  $A$ ,  $B$ ,  $e$ , and  $\rho$  are constant. The output of the STMD after the inhibition  $E(x, y, t, \theta)$  is given by

$$E(x, y, t, \theta) = \iiint D(u, v, t, \psi) \cdot W_s(x - u, y - v) \cdot W_d(\theta - \psi) du dv d\psi. \quad (18)$$

Fig. 6 shows  $E(x, y, t, \theta)$  at pixel  $(x_0, y_0)$  and time  $t_0$  along eight preferred directions  $\theta$ . As can be seen,  $E(x, y, t, \theta)$  is directionally selective. More precisely, the strongest response appears at the motion direction of the small target, i.e.,  $\theta = 0$ . When the preferred direction deviates from  $\theta = 0$ , the neural output decreases significantly and equates to zeros at  $\theta = \pi$  opposite to the motion direction. In addition,  $E(x, y, t, \theta)$  exhibits strong velocity selectivity, as illustrated in Fig. 7. Specifically, the STMD responds to small targets with velocities in a specific range denoted by  $[v_{\min}, v_{\max}]$ , and its output peaks at an optimal velocity denoted by  $v_{\text{opt}}$ . Note that direction and velocity selectivities have been found in real STMD neurons [11].

To determine locations and motion directions of small targets, we compare  $E(x, y, t, \theta)$  with a threshold  $\delta$ . Specially, if  $E(x, y, t, \theta) > \delta$ , then we consider  $(x, y, t, \theta)$  as a positive detection which means a small target moving along direction  $\theta$  is detected at pixel  $(x, y)$  and time  $t$ . However,  $E(x, y, t, \theta)$  may contain a number of false positives induced by small-target-like features in complex backgrounds. To eliminate these false positives, we further compare the variation amount of directional contrast on motion traces of the detected objects, as indicated in [17].

#### E. Prediction Module

The spatial coordinates  $(x_t, y_t)$  and motion directions  $\theta_t$  of the small targets at time  $t$  are obtained by the STMD-based neural network, then fed into the prediction module

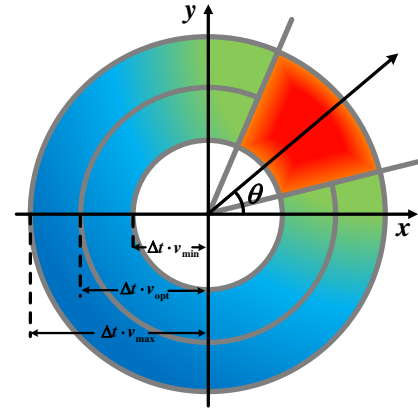


Fig. 8. Potential positions of a small target at time  $t + \Delta t$  where the origin coordinates are  $(x_t, y_t)$  and  $\theta$  denotes the motion direction. The red-ring area represents the positions where the small target would appear with a high probability.

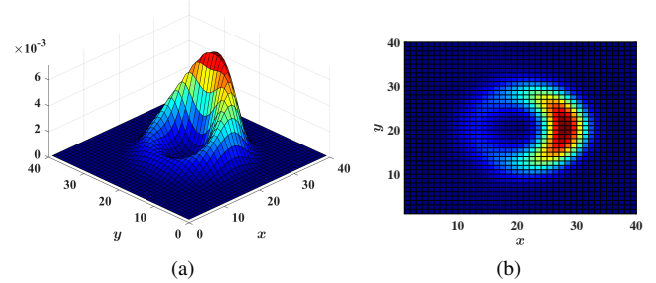


Fig. 9. (a) Three-dimensional and (b) planar representations of a prediction kernel  $W_p(x, y, \theta)$  where  $\theta = 0$ .

to anticipate their future positions. Let  $(x_{t+\Delta t}, y_{t+\Delta t})$  denote the position of a small target at time  $t + \Delta t$ , then it can be described as

$$(x_{t+\Delta t}, y_{t+\Delta t}) = (x_t, y_t) + v_t(\cos(\theta_t + \omega_t), \sin(\theta_t + \omega_t))\Delta t + \varepsilon_t(\cos(\theta_t + \omega_t), \sin(\theta_t + \omega_t))\Delta t \quad (19)$$

where  $v_t$  stands for the velocity of the small target at time  $t$ ;  $\varepsilon_t$  and  $\omega_t$  represent deviations of the velocity and motion direction over the time period  $\Delta t$ , respectively. Note that the STMD is selective to object velocity (see Fig. 7), so  $v_t$  is in the preferred velocity range of the STMD, i.e.,  $v_{\min} \leq v_t \leq v_{\max}$ . Moreover, if the velocity and motion direction of the small target have not significant changes over the period  $\Delta t$ , i.e.,  $\varepsilon_t$  and  $\omega_t$  are all equal to low values in (19), the small target would appear in a ring area with a high probability at time  $t + \Delta t$ , as illustrated in Fig. 8.

Based on the above observation, we define a set of prediction kernels  $W_p(x, y, \theta)$  with various orientations  $\theta$  as

$$W_p(x, y, \theta) = \lambda \cdot \exp \left( -\frac{(x - v_{\text{opt}} \cos \varphi \Delta t)^2}{2\zeta^2} \right) \cdot \exp \left( -\frac{(y - v_{\text{opt}} \sin \varphi \Delta t)^2}{2\zeta^2} \right) \cdot \exp \left( \eta \cos(\varphi - \theta) \right) \quad (20)$$

where  $v_{\text{opt}}$  stands for the optimal velocity of the STMD;  $\varphi$  denotes the angle between the vector  $(x, y)$  and the positive

direction of  $x$ -axis,  $0 \leq \varphi < 2\pi$ ;  $\lambda$  represents normalization factor;  $\zeta$  and  $\eta$  are constant. As can be seen from Fig. 9, the shape of  $W_p(x, y, \theta)$  is similar to that of the future positions in Fig. 8, which displays as a ring structure. In addition, the value of  $W_p(x, y, \theta)$  reveals the probability of a small target appearing at pixel  $(x, y)$ . We further define the predictive gain of the STMD  $F(x, y, t, \theta)$  by

$$F(x, y, t, \theta) = \iint \left\{ \mu E(u, v, t, \theta) + (1 - \mu) F(u, v, t - \Delta t, \theta) \right\} \cdot W_p(x - u, y - v, \theta) du dv \quad (21)$$

where  $E(x, y, t, \theta)$  is the output of the STMD at time  $t$ ;  $F(x, y, t - \Delta t, \theta)$  denotes the predictive gain at time  $t - \Delta t$ ;  $\mu$  is constant and  $0 \leq \mu \leq 1$ . To generate a prediction map, we integrate the predictive gain  $F(x, y, t, \theta)$  in direction domain, that is

$$M(x, y, t) = \int F(x, y, t, \theta) d\theta \quad (22)$$

where  $M(x, y, t)$  denotes the prediction map at time  $t$  which anticipates the locations of small targets at  $t + \Delta t$ . The predictive process is able to facilitate responses of the STMD [21], so we define the facilitated STMD output  $Q(x, y, t, \theta)$  by summing the STMD neural output with the previous prediction gains, that is

$$Q(x, y, t, \theta) = E(x, y, t, \theta) + \beta \cdot \int_{t - \Delta t}^t e^{\kappa \cdot (t - s - \Delta t)} \cdot F(x, y, s, \theta) ds \quad (23)$$

where  $\beta, \kappa$  are constant.

#### F. Memorizer

As shown in Fig. 2, the memorizer collects prediction maps  $M(x, y, t)$  from the prediction module. Let  $\{M(x, y, t) | t \in [0, t_c]\}$  denote the set of the prediction maps where  $t_c$  stands for the current time step. For a new input image at time  $t_c + \Delta t$ , the memorizer provide the prediction map  $M(x, y, t_c)$  to the attention module for determining potential areas.

## IV. EXPERIMENTS AND DISCUSSIONS

### A. Experimental Setup

1) *Data Sets*: We used a simulated data set (Vision Egg) [52] and a real-world data set (RIST) [53] to evaluate the proposed model (apg-STMD) on small target motion detection task. The Vision Egg data set covers a wide variety of synthetic small targets with various luminance, velocity, and size, moving against complex backgrounds. Each synthetic video contains one or multiple small target motion, where sampling frequency is set to 1000 Hz and resolution equates to 500 pixels (horizontal) by 250 pixels (vertical). The RIST data set contains 19 videos captured in the wild using an action camera (GoPro Hero 6) with a resolution  $480 \times 270$  at 240 fps. It covers various challenging scenarios, such as highly cluttered backgrounds, low-contrast targets, sudden camera motion, and bad weather conditions. Each video holds a small moving target whose size ranges between  $3 \times 3$  and  $15 \times 15$  pixels.

TABLE I  
PARAMETERS OF THE PROPOSED VISUAL SYSTEM.

Eq.	Parameters
(2)	$\sigma_1 = 1$
(3)	$\Sigma = \{2.0, 2.5, 3.0, 3.5\}, \Theta = \{0, \pi/4, \pi/2, 3\pi/4\}$
(6)	$n_1 = 2, \tau_1 = 3, n_2 = 6, \tau_2 = 9$
(13)	$\gamma = 3$
(14)	$n_3 = 3, \tau_3 = 15, n_4 = 5, \tau_4 = 25, n_5 = 8, \tau_5 = 40$
(15)	$A = 1, B = 3.5$
(16)	$\sigma_2 = 1.25, \sigma_3 = 2.5, e = 1.2, \rho = 0$
(17)	$\sigma_4 = 1.5, \sigma_5 = 3$
(20)	$\zeta = 2, \eta = 2.5$
(23)	$\kappa = 0.02$

2) *Evaluation Metrics*: To evaluate the performances of small target motion detection methods, we use detection rate ( $D_R$ ) and false alarm rate ( $F_A$ ) that are formulated as follow.

$$D_R = \frac{\text{number of true positives}}{\text{number of actual targets}} \quad (24)$$

$$F_A = \frac{\text{number of false positives}}{\text{number of frames}} \quad (25)$$

where a detection is considered as true positive if its distance to the ground truth is smaller than a threshold (5 pixels);  $D_R$  measures the percentage of the small targets that can be correctly detected while  $F_A$  represents the mean number of false positives in each frame.

3) *Implementation Details*: For given preferred velocity and size ranges of small targets, parameters of the STMD-based neural network are determined by the previous analysis [16]. Parameters  $\zeta, \eta$  that control the shape of the prediction kernel, are properly tuned based on the preferred velocity range. Scales of the attention kernel  $\Sigma$  are determined by the preferred size range to ensure that small targets with optimal size can obtain the largest response after convolution. Multiple STMDs with different preferred velocity and size ranges could be coordinated to detect small objects with unknown velocities and sizes. Other parameters have been set experimentally, but most remained identical for all test image sequences. The parameter settings for the experimental results are listed in Table I. All experiments are tested on MATLAB software platform under a machine that equips with Intel-i7 2.4 GHz CPU, 16 GB memory.

### B. Response Characteristics of the STMD

To reveal response characteristics of the STMD-based neural network, we report its outputs  $E(x, y, t, \theta)$  with respect to different Weber contrast, velocities, widths, and heights. For a target whose size equates to  $w \times h$  pixels, we set its neighboring area as a rectangle with size of  $(w+2d) \times (h+2d)$  pixels where  $d$  is a constant (10 pixels) [16], [17]. Then Weber contrast can be given by

$$\text{Weber contrast} = \frac{|\mu_t - \mu_b|}{255} \quad (26)$$

where  $\mu_t$  denotes average pixel intensity of the target, and  $\mu_b$  represents average pixel intensity in the neighboring area. The

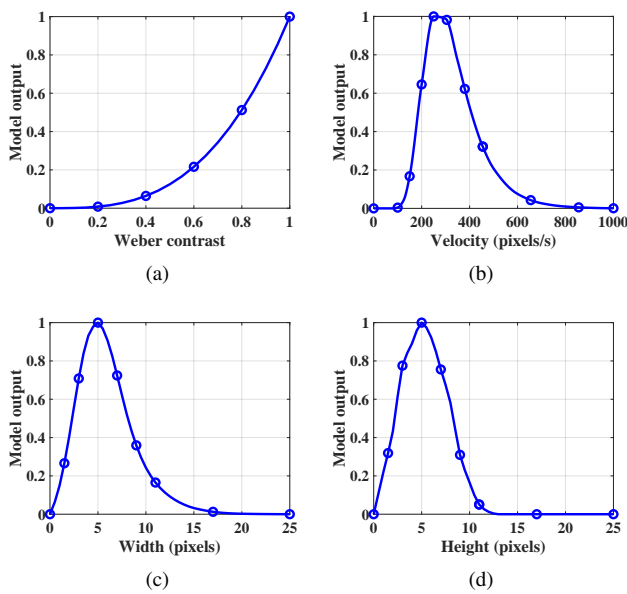


Fig. 10. Outputs of the STMD to a moving target on white background with respect to (a) different Weber contrast, (b) velocities, (c) widths, and (d) heights.

four parameters of the target, i.e., Weber contrast, velocity, width, and height, are initialized to 1, 250 pixels/s, 5 pixels, and 5 pixels, respectively. Four experiments are conducted to analyse the outputs of the STMD with respect to different target parameters, each of which changes one of the parameters while keeping the other three at initial values. The recorded outputs to a moving target on white background are shown in Fig. 10.

As can be seen from Fig. 10(a), the increase in Weber contrast of the target leads to the increase of the STMD output, where the most strongest response is reached at Weber contrast = 1. It can be observed from Fig. 10(b) that the output of the STMD reaches its maximum at 250 spixels/s and is larger than 0 in the interval [100, 800] pixels/s which correspond to the optimal velocity and preferred velocity range of the STMD, respectively. Fig. 10(c) and (d) shows the outputs of the STMD to targets with different widths and heights. As can be seen, the STMD responds to targets whose widths and heights are smaller than 18 and 13 pixels, respectively. In addition, its output peaks at width= 5 pixels and height= 5 pixels.

Fig. 10(a)-(d) provides a good fit to response characteristics of the STMD neurons revealed in biological research [11]–[13], which means the proposed STMD model displays contrast sensitivity, velocity selectivity, width selectivity, and height selectivity, respectively.

### C. Effectiveness of Attention Module

As described in Section III-C, we design an attention module to overcome the heavy dependence of the STMD-based neural network on target contrast against complex background. To validate its effectiveness, we conduct a performance comparison between the STMD-based neural networks with and without an attention module. Fig. 11 shows the input image  $I(x, y, t)$  at time  $t = 760$  ms. As can be seen, two small targets

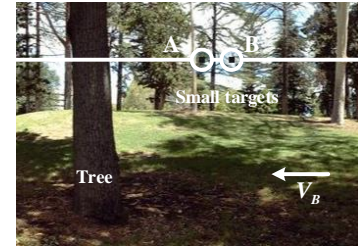


Fig. 11. Input image at time  $t_0 = 760$  ms where two small targets  $A, B$  are moving against the complex background. The background velocity is set as 250 pixels/s, and arrow  $V_B$  denotes its motion direction. The tree is considered as a large object moving with the background at the same velocity.

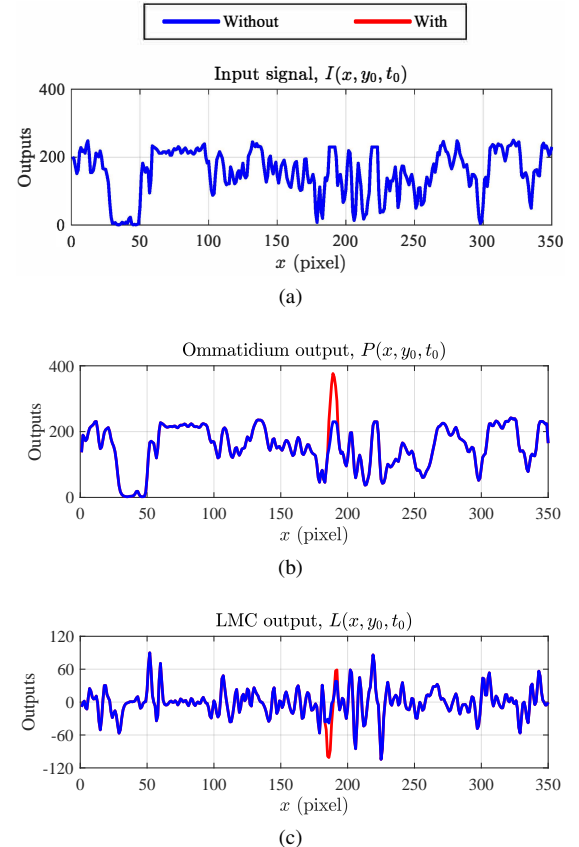


Fig. 12. (a) Input luminance signal  $I(x, y_0, t_0)$  where  $y_0 = 190$  pixels and  $t_0 = 760$  ms. Comparison of (b) Ommatidium outputs  $P(x, y_0, t_0)$ , (c) LMC output  $L(x, y_0, t_0)$  with and without the attention module.

are moving against the complex background where the target  $A$  have much lower contrast to its surrounding background compared to the target  $B$ . In addition, the target  $A$  has relative movement to the background, whereas the target  $B$  remains static relative to the background. To clearly illustrate signal processing, we observe the input luminance signal  $I(x, y_0, t_0)$  with respect to  $x$  by setting  $y_0 = 190$  pixels in Fig. 12(a), and then analyse its resulting neural outputs with and without the attention module in Fig. 12(b), (c) and Fig. 13.

Fig. 12(b) shows the outputs of the ommatidium with and without the attention module. As can be seen, the ommatidium smooths the input luminance signal by applying Gaussian blur. The attention module further enhances the contrast of the small target  $A$  to surrounding background by adding its convolution

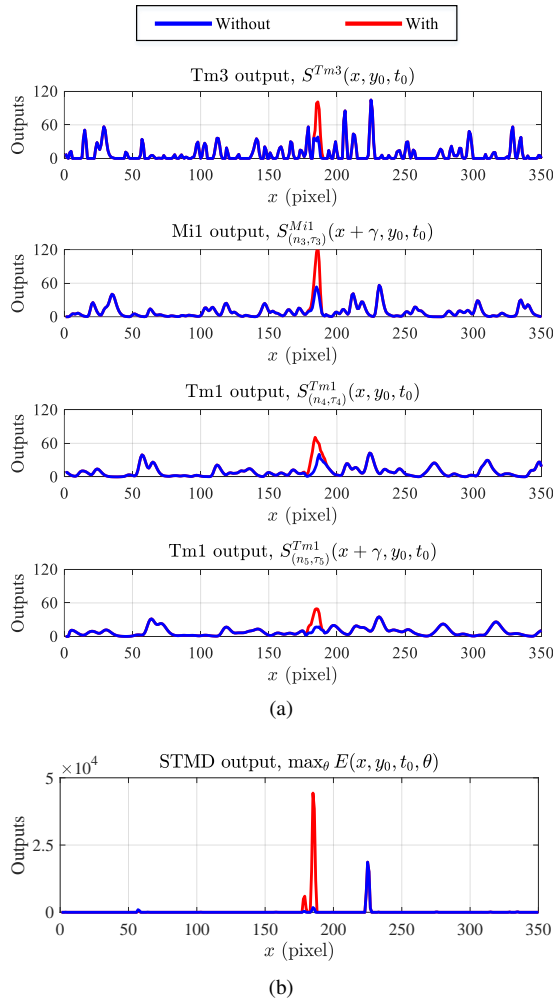


Fig. 13. Comparison of (a) medulla neural outputs, (b) STMD output  $E(x, y_0, t_0)$  with and without the attention module.

output on the smoothed input signal. In comparison, the target *B* does not receive attention, because it remains static relative to the background and is regarded as a part of the background. As shown in Fig. 12(c), the LMC computes luminance changes of each pixel over time, where its positive output means the increase in luminance while the negative output reveals the luminance decrease. Since the contrast of the small target *A* has been strengthened, it induces much more significant luminance changes with respect to time.

Fig. 13(a) illustrates the outputs of four medulla neurons with and without the attention module. As can be seen,  $S^{Tm3}(x, y_0, t_0)$  corresponds to the positive component of the LMC output;  $S^{Mi1}_{(n_3, \tau_3)}(x + \gamma, y_0, t_0)$  is a time-delay version of  $S^{Tm3}(x, y_0, t_0)$  with a spatial shift  $\gamma$  along direction  $\theta = 0$  where time-delay length and order are set as  $\tau_3$  and  $n_3$ , respectively;  $S^{Tm1}_{(n_4, \tau_4)}(x, y_0, t_0)$  is a time-delay version of the negative component of the LMC output where time-delay length and order are equal to  $\tau_4$  and  $n_4$ , respectively;  $S^{Tm1}_{(n_5, \tau_5)}(x + \gamma, y_0, t_0)$  is another time-delay version of the negative component of the LMC output with a spatial shift  $\gamma$  along direction  $\theta = 0$ . Furthermore, the medulla neural outputs at the position of the target *A* are all strengthened

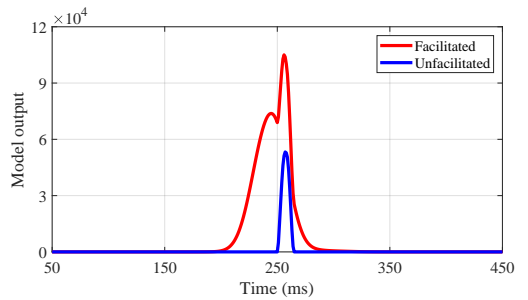


Fig. 14. Unfacilitated and facilitated STMD neural responses to a small target at a pixel with respect to time.

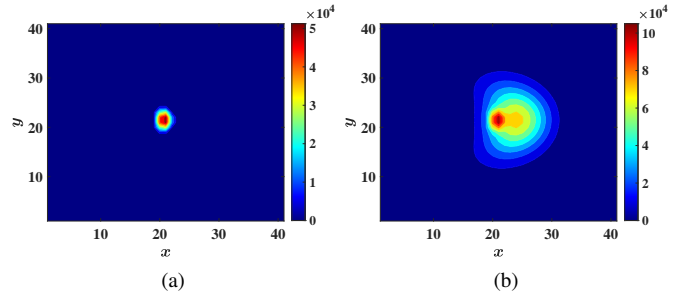


Fig. 15. Planar representations of (a) Unfacilitated and (b) facilitated STMD neural responses to a small target where direction  $\theta$  and time  $t$  are equal to  $\theta = 0$  and  $t = 320$  ms, respectively.

by the attention module, whereas the neural outputs at other positions remain unchanged. These four neural outputs that have been aligned in the time domain by time delay and spatial shift, are multiplied together to define the STMD output. Fig. 13(b) shows the maximal output of the STMD over the direction  $\theta$ , i.e.,  $\max_{\theta} E(x, y_0, t_0, \theta)$ . It can be observed that the attention module significantly enhances the STMD response to the low-contrast target *A*, while maintaining response to the high-contrast target *B* that moves relatively static to the background. Note that the STMD-based neural networks with and without attention module all exhibit no response to the large objects, i.e., the tree.

#### D. Facilitation Effect of Prediction Module

Predictive mechanism is able to boost the STMD neural responses, enhance contrast sensitivity and direction selectivity, and facilitate the pursuit of occluded objects, as revealed in biological research [21]. To validate the above facilitation effect of the proposed prediction module, we conduct four experiments in the following subsections.

1) *Facilitation in Neural Responses*: We first compare the STMD neural outputs with and without facilitation where the unfacilitated output  $E(x, y, t, \theta)$  and the facilitated output  $Q(x, y, t, \theta)$  are defined by (18) and (23), respectively. As can be seen from Fig. 14, the unfacilitated STMD response builds up rapidly over 7–8 ms to its peak. However, the facilitated response shows a slow build-up lasting roughly 50 ms before reaching its maximum which is about twice as strong as that of the unfacilitated response. Fig. 15 shows the STMD responses with and without facilitation over spatial domain. Compared to

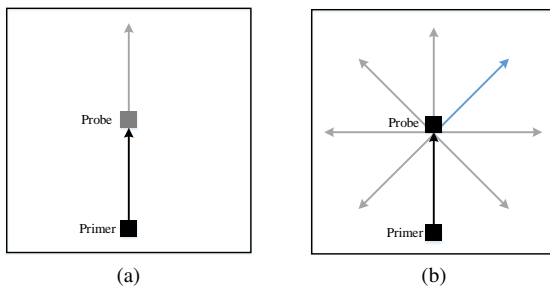


Fig. 16. (a)-(b) Schematics of the Primer & Probe test for validation of facilitatory effect in contrast sensitivity and direction selectivity, respectively.

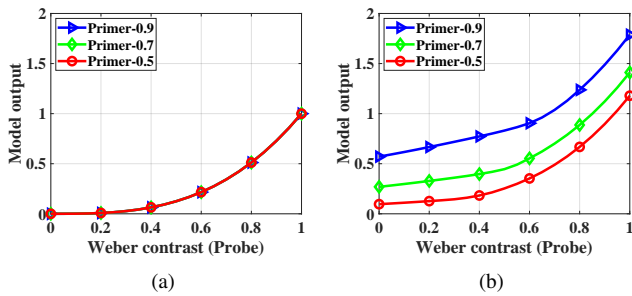


Fig. 17. (a) Unfacilitated and (b) facilitated STMD outputs to the probe with different Weber contrast, preceded by varying-contrast primer.

the unfacilitated response, the prediction module enhances the local STMD responses in a broad region ahead of the target motion direction.

2) *Facilitation in Contrast Sensitivity*: To validate the facilitatory effect in contrast sensitivity, we conduct a Primer & Probe experiment as shown in Fig. 16(a). Specifically, the input video displays a small target moving along a long path which are separated into two components called the primer and the probe, respectively. The primer segment is used to induce spatial facilitation, while the second segment, the probe, is used to record model outputs. We change the Weber contrast of the primer and probe, respectively, and then record the STMD outputs with and without facilitation to the probe. As can be seen from Fig. 17, the STMD output without facilitation remains unchanged when the contrast of the primer increases. However, for any given contrast of the probe, the STMD output with facilitation shows a significant increase with the growth in the contrast of the primer.

3) *Facilitation in Direction Selectivity*: To validate the facilitatory effect in direction selectivity, we conduct another Primer & Probe experiment as shown in Fig. 16(b). Specifically, we fix Weber contrast of the primer and probe, then change the angular offset between the primer path and probe path, finally record the STMD outputs with and without facilitation to the probe. As can be seen from Fig. 18, the motion of the primer shows little effect on the STMD responses without facilitation to the probe. More precisely, the unfacilitated STMD responses along eight directions are equal, regardless of the primer's motion direction. However, the prediction module facilitates the STMD response maximally in the motion direction of the primer. The direction tuning is

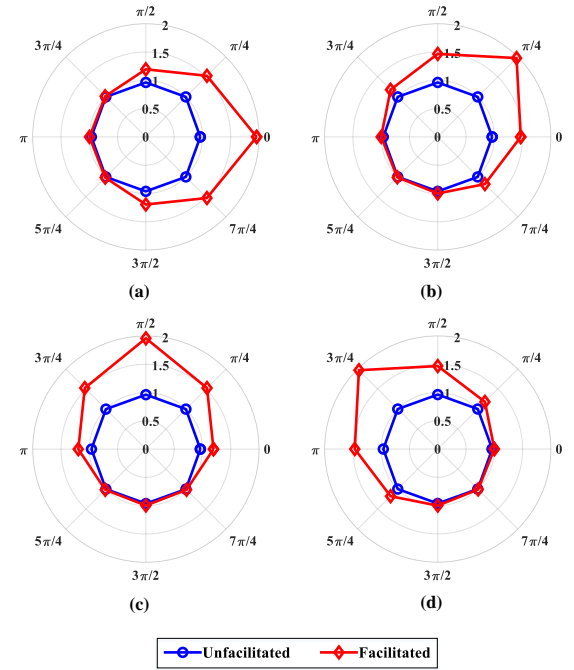


Fig. 18. Unfacilitated and facilitated STMD outputs to the probes moving along eight directions  $\theta \in \{0, \frac{\pi}{4}, \frac{\pi}{2}, \frac{3\pi}{4}, \pi, \frac{5\pi}{4}, \frac{3\pi}{2}, \frac{7\pi}{4}\}$  when the motion direction of the primer is set to (a) 0, (b)  $\frac{\pi}{4}$ , (c)  $\frac{\pi}{2}$ , (d)  $\frac{3\pi}{4}$ , respectively.

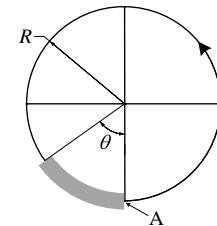


Fig. 19. Representation of small target motion in  $xy$  plane where the target is moving counterclockwise along the circular path of radius  $R$ . During the revolution, the target is occluded (gray thick line) where the angle of the occlusion is given by  $\theta$  and  $A$  denotes the end point of the occlusion.

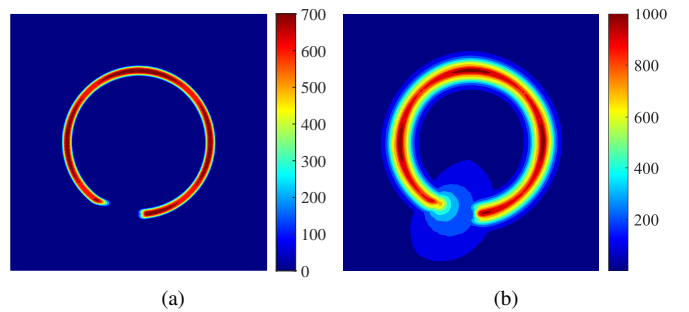


Fig. 20. Planar representations of (a) unfacilitated and (b) facilitated STMD outputs when the radius  $R$  and the occlusion angle  $\theta$  is set to 50 pixels and  $30^\circ$ , respectively. For better visualization, square root of the output is displayed.

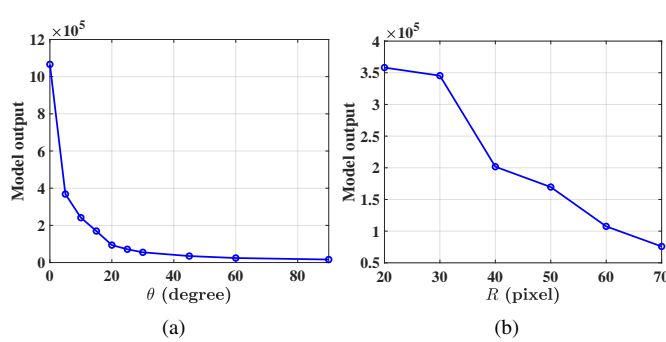
also shifted to match the motion direction of the primer.

4) *Facilitation in Pursuit of Occluded Objects*: To validate the facilitatory effect of the prediction module in smooth pursuit of a moving target that is transiently occluded, we conduct an experiment shown in Fig. 19. As can be seen,

TABLE II

DETAILS OF THE SYNTHETIC IMAGE SEQUENCES THAT ARE CATEGORIZED INTO FIVE GROUPS IN TERMS OF FIVE DIFFERENT IMAGE PARAMETERS.

Image parameter	Initial sequence	Group 1	Group 2	Group 3	Group 4	Group 5
Target velocity (pixels/s)	250	<b>100 ~ 500</b>	250	250	250	250
Target size (pixels $\times$ pixels)	$5 \times 5$	$5 \times 5$	<b>1 <math>\times</math> 1 ~ 12 <math>\times</math> 12</b>	$5 \times 5$	$5 \times 5$	$5 \times 5$
Target luminance	25	25	25	<b>0 ~ 75</b>	25	25
Background velocity (pixels/s)	250	250	250	250	<b>0 ~ 500</b>	<b>0 ~ 500</b>
Background motion direction	leftward	leftward	leftward	leftward	leftward	<b>rightward</b>
Background Image	Fig.22	Fig.22	Fig.22	Fig.22	Fig.22	Fig.22

Fig. 21. Outputs of the STMD with facilitation at pixel A, i.e., the end point of the occlusion, with respect to (a) occlusion angle  $\theta$  and (b) radius  $R$ .

the input video contains a small target with velocity of 250 pixels/s moving counterclockwise on a circular path of radius  $R$ . The target is occluded on part of the circular path where the occlusion angle is set as  $\theta$ .

Fig. 20 shows the unfacilitated and facilitated STMD outputs on spatial domain when the radius  $R$  and the occlusion angle  $\theta$  are equal to 50 pixels and  $30^\circ$ , respectively. As can be seen, both the unfacilitated and facilitated STMD responses form a gaped circular path. However, the width of the circle path formed by the facilitated output is much wider than that of the unfacilitated output. In addition, the facilitated STMD output still spreads forward after the small target disappears. However, the unfacilitated output is close to zero during the occlusion. We further reveal the relationship between the STMD output after the occlusion (pixel  $A$ ) and occlusion angle  $\theta$  and radius  $R$ , respectively. As shown in Fig. 21, the increase in occlusion angle  $\theta$  and radius  $R$  will induce the decrease in the STMD output propagated to pixel  $A$ , which means that prediction precision will decrease with the increase in occlusion period.

#### E. Evaluation on Synthetic and Real-World Data Sets

We first conduct performance evaluation on synthetic videos with a single small target motion but with varying image parameters, including target velocity, target size, target luminance, background velocity, and background motion direction (Vision Egg data set [52]). Then we further validate effectiveness of the proposed model on synthetic videos that contains multiple small targets moving against different background images. Finally, we conduct experiments on the real-world data set, i.e., RIST data set [53]. In each experiment, the



Fig. 22. Representative frame of the input video where a small target is moving against the complex background.

receiver operating characteristics (ROC) curves are computed to quantitatively evaluate the performance of the proposed model and baseline methods, including DSTMD [16], ESTMD [14], and STMD Plus [17].

1) *Performances on Synthetic Videos with Varying Parameters*: We categorize synthetic image sequences into five groups based on target velocity, target size, target luminance, background velocity, and background motion direction. The details of the five groups of image sequences are listed in Table II and a representative frame of the input image sequence is shown in Fig. 22. The proposed model significantly outperforms the three baseline methods by a large margin on the initial image sequence in terms of the ROC curve, as illustrated in Fig. 23(a). Specifically, for a fixed false alarm rate, the proposed model has the highest detection rate that is close to 1, compared to other three methods.

Fig. 23(b)-(f) illustrates detection rates of all four models with respect to target velocity, target size, target luminance, background velocity, and background motion direction, respectively, where false alarm rates are fixed to 1 for quantitative comparison. As can be seen from Fig. 23(b), the proposed model consistently performs best under all target velocities. Its detection rate equates to 1 for target velocity ranging from 200 to 350 pixels/s, and experiences a slight decrease when velocity exceeds this preferred range. In Fig. 23(c), we can find that all the models have a preferred size range roughly between  $3 \times 3$  and  $8 \times 8$  pixels where all the models reach their maximal detection rates. Compared to the baseline methods, the proposed model has the highest detection rate for all target sizes. In addition, it maintains a high detection rate ( $> 0.5$ ) for targets whose sizes exceed the preferred range, whereas the baseline methods experience a sharp decrease to 0 in detection rate. As displayed in Fig. 23(d), the proposed model consistently outperforms the baseline methods

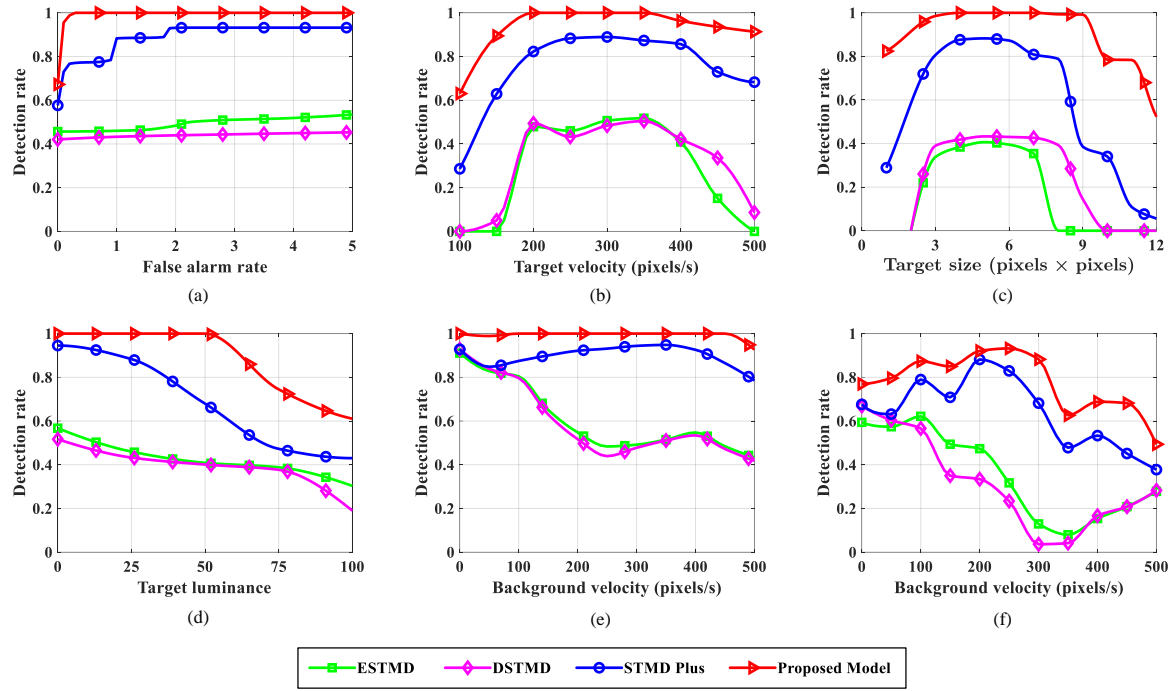


Fig. 23. (a) ROC curves of the proposed model and three baseline methods on the initial image sequence. (b)-(f) Detection rates under the fixed false alarm rate  $F_A = 1$  with respect to (b) target size, (c) target luminance, (d) target velocity, (e) background velocity (leftward motion), and (f) background velocity (rightward motion). The proposed model consistently performs better than other methods across all the image sequences.

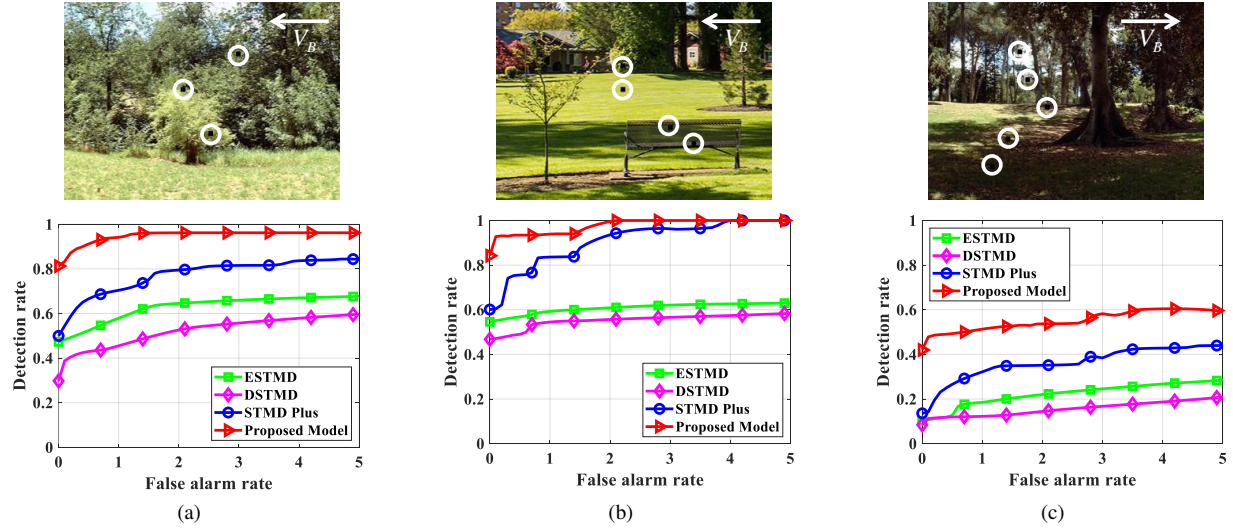


Fig. 24. (a)-(c) Representative frames of the three synthetic videos that hold multiple small targets moving against complex backgrounds and corresponding ROC curves of the proposed model and three baseline methods. The proposed model consistently performs best among four different methods for multiple small target detection against different background images.

for different levels of luminance. Moreover, the increase in target luminance will lead to the performance degradation of the baseline methods. However, the propose model maintains superior performance and its detection rate remains stable at 1 for target luminance lower than 50. Fig. 23(e) and (f) compares the performance of the four models under different background velocities. In comparison to the baseline methods, the proposed model clearly improve detection rates regardless of background velocities.

2) *Performances on Synthetic Videos with Multiple Small Targets:* Fig. 24(a)-(c) reports the performance comparison between the proposed model and baseline methods in terms of the ROC curves for synthetic videos that holds three, four, and five small targets, respectively. As it is shown, the proposed model yields much better performance than the three baseline methods on all the three videos. Note that the detection rate of a model in Fig. 24(a) is clearly higher than that in Fig. 24(c). This is because the background image of Fig. 24(c) contains numerous shaded areas where small targets are easily occluded

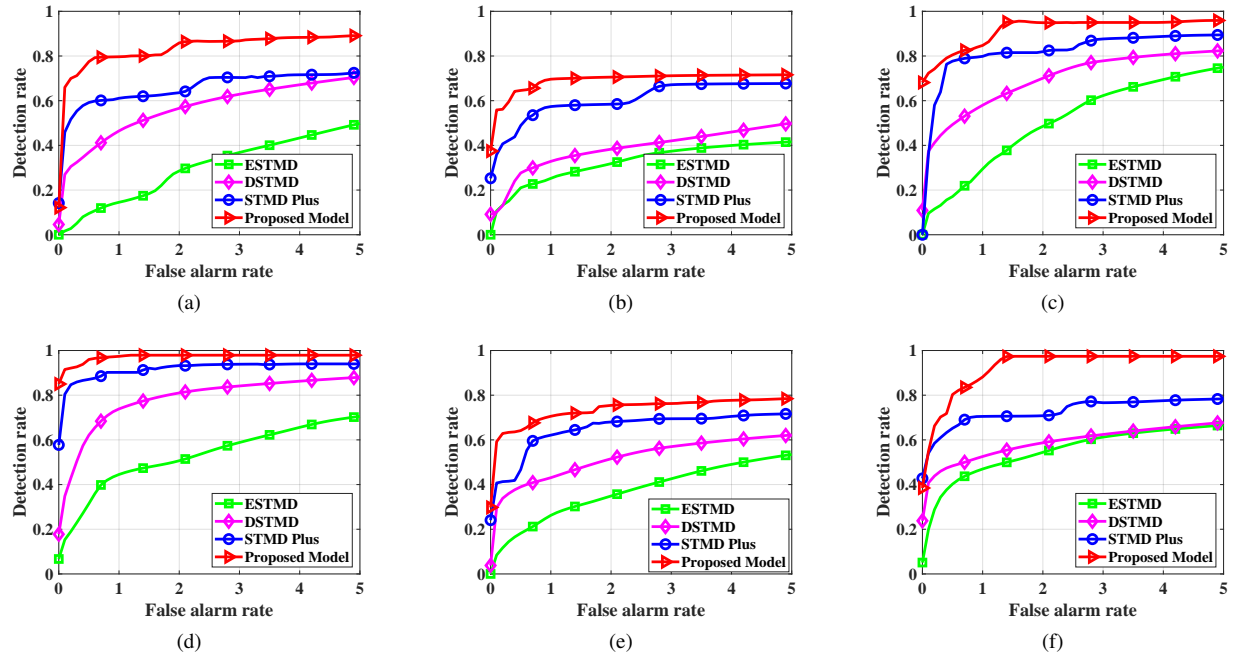


Fig. 25. (a)-(f) ROC curves of the proposed model and three baseline methods on six real videos corresponding to GX010071, GX010307, GX010315, GX010321, GX010327, GX010336 in the RIST data set, respectively. The proposed model consistently achieves the best results on all real videos.

or exhibit extremely low contrast to surrounding background.

3) *Performances on Real Data Set*: We randomly select six real-world videos from the RIST data set, each of which holds a small target with varying contrast to complex background in challenging scenario. Fig. 25(a)-(f) reports the ROC curves of the proposed model and the three baseline methods on the six videos whose numbers are listed in the caption, respectively. As can be seen, the proposed model achieves much improvement over the three baseline methods on all six real-world videos. For any given false alarm rate, the proposed model always obtains higher detection rate compared to the ESTMD, DSTMD, and STMD Plus.

## V. CONCLUSION

This article proposes a attention and prediction guided visual system to detect small targets in complex natural environments. To mitigate the heavy dependency on target contrast against the background, the proposed visual system introduces an attention module, a STMD-based neural network, and a prediction module, which are arranged in a recurrent architecture. The attention module is designed to search for potential small targets in predicted areas over the input image and enhance their contrast to neighboring backgrounds. The STMD-based neural network is devised to take the contrast-enhanced image as input and detect small moving targets using both motion information and directional contrast. The prediction module is proposed to anticipate future positions of the detected small targets and generate a prediction for next time step. The proposed visual system significantly improves the performance for small target detection in complex natural environment where small targets always exhibit extremely low contrast. The experiments validate its superiority, which perform the best on both synthetic and real-world data sets.

## REFERENCES

- [1] [Online]. Available: [https://www.youtube.com/watch?v=wphymrmtkjI&list=FL\\_OHabe8rogCpinac5KHGYA&index=1](https://www.youtube.com/watch?v=wphymrmtkjI&list=FL_OHabe8rogCpinac5KHGYA&index=1), accessed Aug. 11, 2020.
- [2] I. Saleemi and M. Shah, "Multiframe many-many point correspondence for vehicle tracking in high density wide area aerial videos," *Int. J. Comput. Vision*, vol. 104, no. 2, pp. 198–219, Sep. 2013.
- [3] S. Javed, A. Mahmood, S. Al-Maadeed, T. Bouwmans, and S. K. Jung, "Moving object detection in complex scene using spatiotemporal structured-sparse rpca," *IEEE Trans. Image Process.*, vol. 28, no. 2, pp. 1007–1022, Oct. 2018.
- [4] D. Fortun, P. Bouthemy, and C. Kervrann, "Optical flow modeling and computation: a survey," *Comput. Vis. Image Underst.*, vol. 134, pp. 1–21, May 2015.
- [5] J. Redmon, S. Divvala, R. Girshick, and A. Farhadi, "You only look once: Unified, real-time object detection," in *Proc. IEEE Conf. Comput. Vis. Pattern Recognit.*, June 2016, pp. 779–788.
- [6] J. Tang, Y. Tian, P. Zhang, and X. Liu, "Multiview privileged support vector machines," *IEEE Trans. Neural Netw. Learn. Syst.*, vol. 29, no. 8, pp. 3463–3477, Aug. 2017.
- [7] J. Zhang, Z.-h. Zhan, Y. Lin, N. Chen, Y.-j. Gong, J.-h. Zhong, H. S. Chung, Y. Li, and Y.-h. Shi, "Evolutionary computation meets machine learning: A survey," *IEEE Computational Intelligence Magazine*, vol. 6, no. 4, pp. 68–75, Oct. 2011.
- [8] H. Wang, Q. Fu, H. Wang, P. Baxter, J. Peng, and S. Yue, "A bioinspired angular velocity decoding neural network model for visually guided flights," *Neural Netw.*, vol. 136, pp. 180–193, Apr. 2021.
- [9] X. Sun, S. Yue, and M. Mangan, "A decentralised neural model explaining optimal integration of navigational strategies in insects," *Elife*, vol. 9, p. e54026, 2020.
- [10] Q. Fu, H. Wang, C. Hu, and S. Yue, "Towards computational models and applications of insect visual systems for motion perception: A review," *Artif. Life*, vol. 25, no. 3, pp. 263–311, 2019.
- [11] K. Nordström, P. D. Barnett, and D. C. O'Carroll, "Insect detection of small targets moving in visual clutter," *PLoS Biol.*, vol. 4, no. 3, p. e54, Feb. 2006.
- [12] P. D. Barnett, K. Nordström, and D. C. O'Carroll, "Retinotopic organization of small-field-target-detecting neurons in the insect visual system," *Curr. Biol.*, vol. 17, no. 7, pp. 569–578, Apr. 2007.
- [13] K. Nordström, "Neural specializations for small target detection in insects," *Curr. Opin. Neurobiol.*, vol. 22, no. 2, pp. 272–278, Apr. 2012.
- [14] S. D. Wiederman, P. A. Shoemaker, and D. C. O'Carroll, "A model for the detection of moving targets in visual clutter inspired by insect physiology," *PLoS One*, vol. 3, no. 7, pp. 1–11, Jul. 2008.

- [15] S. D. Wiederman and D. C. O'Carroll, "Biologically inspired feature detection using cascaded correlations of off and on channels," *J. Artif. Intell. Soft Comput. Res.*, vol. 3, no. 1, pp. 5–14, Dec. 2013.
- [16] H. Wang, J. Peng, and S. Yue, "A directionally selective small target motion detecting visual neural network in cluttered backgrounds," *IEEE Trans. Cybern.*, vol. 50, no. 4, pp. 1541–1555, Apr. 2020.
- [17] H. Wang, J. Peng, X. Zheng, and S. Yue, "A robust visual system for small target motion detection against cluttered moving backgrounds," *IEEE Trans. Neural Netw. Learn. Syst.*, vol. 31, no. 3, pp. 839–853, Mar. 2020.
- [18] V. Nityananda, "Attention-like processes in insects," *Proc. R. Soc. B*, vol. 283, no. 1842, p. 20161986, Nov. 2016.
- [19] E. Schröger, S. A. Kotz, and I. SanMiguel, "Bridging prediction and attention in current research on perception and action," *Brain Research*, vol. 1626, pp. 1–13, Nov. 2015.
- [20] Z. M. Bagheri, C. G. Donohue, and J. M. Hemmi, "Evidence of predictive selective attention in fiddler crabs during escape in the natural environment," *J. Exp. Biol.*, vol. 223, no. 21, Nov. 2020.
- [21] S. D. Wiederman, J. M. Fabian, J. R. Dunbier, and D. C. O'Carroll, "A predictive focus of gain modulation encodes target trajectories in insect vision," *Elife*, vol. 6, p. e26478, Jul. 2017.
- [22] F. C. Rind, S. Wernitznig, P. Pölt, A. Zankel, D. Gütl, J. Sztarker, and G. Leitinger, "Two identified looming detectors in the locust: ubiquitous lateral connections among their inputs contribute to selective responses to looming objects," *Sci. Rep.*, vol. 6, no. 1, pp. 1–16, Oct. 2016.
- [23] F. C. Rind and D. Bramwell, "Neural network based on the input organization of an identified neuron signaling impending collision," *J. Neurophysiol.*, vol. 75, no. 3, pp. 967–985, Mar. 1996.
- [24] M. S. Maisak, J. Haag, G. Ammer, E. Serbe, M. Meier, A. Leonhardt, T. Schilling, A. Bahl, G. M. Rubin, A. Nern *et al.*, "A directional tuning map of drosophila elementary motion detectors," *Nature*, vol. 500, no. 7461, pp. 212–216, Aug. 2013.
- [25] M. Perry, N. Konstantinides, F. Pinto-Teixeira, and C. Desplan, "Generation and evolution of neural cell types and circuits: insights from the drosophila visual system," *Annual review of genetics*, vol. 51, pp. 501–527, 2017.
- [26] S. Yue and F. C. Rind, "Collision detection in complex dynamic scenes using an lgmd-based visual neural network with feature enhancement," *IEEE Trans. Neural Netw.*, vol. 17, no. 3, pp. 705–716, May 2006.
- [27] ———, "Redundant neural vision systems-competing for collision recognition roles," *IEEE Trans. Auton. Mental Develop.*, vol. 5, no. 2, pp. 173–186, Apr. 2013.
- [28] C. Hu, F. Arvin, C. Xiong, and S. Yue, "Bio-inspired embedded vision system for autonomous micro-robots: the lgmd case," *IEEE Trans. Cogn. Develop. Syst.*, vol. 9, no. 3, pp. 241–254, Sep. 2016.
- [29] Q. Fu, C. Hu, J. Peng, F. C. Rind, and S. Yue, "A robust collision perception visual neural network with specific selectivity to darker objects," *IEEE Trans. Cybern.*, vol. 50, no. 12, pp. 5074–5088, Dec. 2019.
- [30] J. Zhao, C. Hu, C. Zhang, Z. Wang, and S. Yue, "A bio-inspired collision detector for small quadcopter," in *2018 International Joint Conference on Neural Networks (IJCNN)*. IEEE, 2018, pp. 1–7.
- [31] L. Salt, D. Howard, G. Indiveri, and Y. Sandamirskaya, "Parameter optimization and learning in a spiking neural network for uav obstacle avoidance targeting neuromorphic processors," *IEEE Trans. Neural Netw. Learn. Syst.*, vol. 31, no. 9, pp. 3305–3318, Oct. 2019.
- [32] H. Eichner, M. Joesch, B. Schnell, D. F. Reiff, and A. Borst, "Internal structure of the fly elementary motion detector," *Neuron*, vol. 70, no. 6, pp. 1155–1164, Jun. 2011.
- [33] A. J. Cope, C. Sabo, K. Gurney, E. Vasilaki, and J. A. Marshall, "A model for an angular velocity-tuned motion detector accounting for deviations in the corridor-centering response of the bee," *PLoS Comput. Biol.*, vol. 12, no. 5, p. e1004887, 2016.
- [34] O. J. Bertrand, J. P. Lindemann, and M. Egelhaaf, "A bio-inspired collision avoidance model based on spatial information derived from motion detectors leads to common routes," *PLoS Comput. Biol.*, vol. 11, no. 11, p. e1004339, 2015.
- [35] J. M. Missler and F. A. Kamangar, "A neural network for pursuit tracking inspired by the fly visual system," *Neural Netw.*, vol. 8, no. 3, pp. 463–480, 1995.
- [36] V. Nityananda and J. G. Patrick, "Bumblebee visual search for multiple learned target types," *J. Exp. Biol.*, vol. 216, no. 22, pp. 4154–4160, Oct. 2013.
- [37] P. Sareen, R. Wolf, and M. Heisenberg, "Attracting the attention of a fly," *Proc. Natl. Acad. Sci. U.S.A.*, vol. 108, no. 17, pp. 7230–7235, Apr. 2011.
- [38] V. Mnih, N. Heess, A. Graves *et al.*, "Recurrent models of visual attention," *Advances in neural information processing systems*, vol. 27, pp. 2204–2212, 2014.
- [39] Z. Yang, X. He, J. Gao, L. Deng, and A. Smola, "Stacked attention networks for image question answering," in *Proceedings of the IEEE conference on computer vision and pattern recognition*, 2016, pp. 21–29.
- [40] A. Vaswani, N. Shazeer, N. Parmar, J. Uszkoreit, L. Jones, A. N. Gomez, Ł. Kaiser, and I. Polosukhin, "Attention is all you need," in *Advances in neural information processing systems*, 2017, pp. 5998–6008.
- [41] L. Chen, H. Zhang, J. Xiao, L. Nie, J. Shao, W. Liu, and T.-S. Chua, "Sca-cnn: Spatial and channel-wise attention in convolutional networks for image captioning," in *Proceedings of the IEEE conference on computer vision and pattern recognition*, 2017, pp. 5659–5667.
- [42] M. Mischiati, H.-T. Lin, P. Herold, E. Imler, R. Olberg, and A. Leonardo, "Internal models direct dragonfly interception steering," *Nature*, vol. 517, no. 7534, pp. 333–338, Dec. 2015.
- [43] J. F. Kooij, F. Flohr, E. A. Pool, and D. M. Gavrila, "Context-based path prediction for targets with switching dynamics," *Int. J. Comput. Vis.*, vol. 127, no. 3, pp. 239–262, 2019.
- [44] M. Luber, J. A. Stork, G. D. Tipaldi, and K. O. Arras, "People tracking with human motion predictions from social forces," in *IEEE Int. Conf. Robot. Autom. (ICRA)*. IEEE, 2010, pp. 464–469.
- [45] F. Stulp, J. Grizou, B. Busch, and M. Lopes, "Facilitating intention prediction for humans by optimizing robot motions," in *IEEE/RSJ international conference on intelligent robots and systems (IROS)*. IEEE, 2015, pp. 1249–1255.
- [46] R. Behnia, D. A. Clark, A. G. Carter, T. R. Clandinin, and C. Desplan, "Processing properties of on and off pathways for drosophila motion detection," *Nature*, vol. 512, no. 7515, p. 427, Aug. 2014.
- [47] E. J. Warrant, "The remarkable visual capacities of nocturnal insects: vision at the limits with small eyes and tiny brains," *Philos. Trans. R. Soc. B*, vol. 372, no. 1717, p. 20160063, Apr. 2017.
- [48] L. Freifeld, D. A. Clark, M. J. Schnitzer, M. A. Horowitz, and T. R. Clandinin, "Gabaergic lateral interactions tune the early stages of visual processing in drosophila," *Neuron*, vol. 78, no. 6, pp. 1075–1089, Jun. 2013.
- [49] S.-y. Takemura, A. Bharioke, Z. Lu, A. Nern, S. Vitaladevuni, P. K. Rivlin, W. T. Katz, D. J. Olbris, S. M. Plaza, P. Winston *et al.*, "A visual motion detection circuit suggested by drosophila connectomics," *Nature*, vol. 500, no. 7461, p. 175, Aug. 2013.
- [50] G. Wang, C. Lopez-Molina, and B. De Baets, "Blob reconstruction using unilateral second order gaussian kernels with application to high-iso long-exposure image denoising," in *Proceedings of the IEEE International Conference on Computer Vision (ICCV)*, Oct 2017.
- [51] B. De Vries and J. C. Príncipe, "A theory for neural networks with time delays," in *Proc. NIPS*, 1990, pp. 162–168.
- [52] A. D. Straw, "Vision egg: an open-source library for realtime visual stimulus generation," *Front. Neuroinf.*, vol. 2, no. 4, Nov. 2008.
- [53] *RIST Data Set*. [Online]. Available: <https://sites.google.com/view/hongxinwang-personalsite/download>, accessed Apr. 6, 2020.